ACSNANO

www.acsnano.org

ARTICLE

Unusually Strong Biexciton Repulsion Detected in Quantum Confined $CsPbBr_3$ Nanocrystals with Two and Three Pulse Femtosecond Spectroscopy

Jayanta Dana, Tal Binyamin, Lioz Etgar, and Sanford Ruhman*

Cite This: https://doi.org/10.1021/acsnano.1c02123

Read Online

ACCESS | Metrics & More | Article Recommendations | Supporting Information

ABSTRACT: Transient absorption measurements were conducted on pristine and monoexciton saturated $CsPbBr_3$ nanocrystals varying in size within the regime of a strong quantum confinement. Once the difference spectra were translated to absolute transient changes in absorption cross section, a single exciton is shown to completely bleach the band edge absorption peak and induce a new absorption roughly two times weaker ~100 meV to the blue. Difference spectra obtained during Auger recombination of biexciton demonstrate that the addition of a second exciton, rather than double the effect of a first, bleaches the blue-induced absorption band without producing a net stimulated emission at the band edge. Accompanied by high time resolution transient absorption spectra pumping at the lowest exciton band, these results identify the blue-induced absorption as the second transition to $1S_e1S_h$ which is shifted in energy due to unusually strong and promptly rising biexciton repulsion. Possible mechanisms giving rise to this repulsion and prospects for applying it to enhance optical gain applications of these particles are discussed.

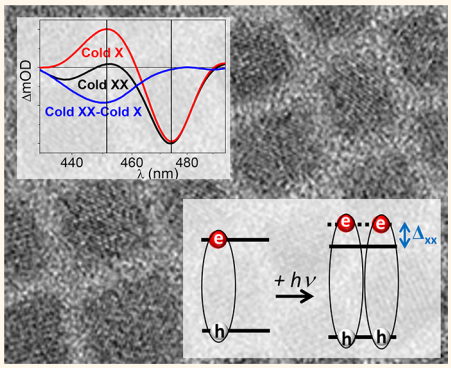

KEYWORDS: *perovskite, quantum confined, biexciton repulsion, spectator exciton, stimulated emission*

The intense optical transition between discrete band edge states which develops in quantum confined (QC) semiconductor nanocrystals (NCs)[1,2] also coined nanodots (NDs) is the vehicle for their application in photonics and optoelectronics.[3−6] The low state degeneracies and immense transition dipoles involved allow the observation of diverse linear and nonlinear effects at relatively low field intensities. As an example, intensity of the band edge (BE) absorption is exquisitely sensitive to exciton occupation in NDs, and the bleach amplitude of this feature in transient absorption (TA) serves as an "exciton counter" for the first few excitations per particle. The dependence of BE bleach amplitudes in TA on pump−probe delay and on pump intensity has accordingly served to quantify single particle absorption cross sections,[7−9] to monitor Auger recombination dynamics,[10,11] and to determine highest occupied molecular orbital (HOMO) and lowest unoccupied molecular orbital (LUMO) state degeneracies.[12−14] The extreme utility of giant oscillator strength BE transitions afforded by quantum confinement in semiconductor QDs and attractive qualities of inorganic and hybrid lead halide perovskite semiconductors, which include ease of preparation and strong defect resistance, have driven a vigorous effort for preparing stable colloidal NDs from these materials. This has however proven challenging, and much of their investigation has dealt with bulk-like MLHP particles. While this can be judiciously used to record bulk photophysics of these materials,[15,16] a means of preparing NCs below the QC limit is essential for realizing their full potential.

Recent synthetic advances have enabled production of QC crystals of all inorganic metal lead halide perovskites (MLHP)[17−19] with tight size distributions which exhibit unique TA signatures.[20] As in other QD samples, above band gap excitation leads to rapid bleaching at the BE accompanied by an induced absorption at longer wavelengths (A1), both often assigned to biexciton interaction of the pump and probe related excitons.[7,21] Cooling of hot carriers causes a typical rise in the BE bleach and decay of A1.[22,23] But unlike other semiconductor materials, carrier cooling of a hot exciton

Received: March 11, 2021
Accepted: May 6, 2021

in MLHP NCs also causes an absorption band to rise in between the $1S_e1S_h$ and $1P_e1P_h$ exciton peaks (X1 and X2 in Figure 1), henceforth coined A2.[20] First reported by Son and co-workers, its appearance was assigned to exciton-induced activation of a forbidden transition to a mixed angular momentum state where the envelope functions of electron and hole are uneven. The delayed rise of this feature over several hundreds of fs was taken to show that it is activated by a time-consuming polaron like deformation of the NC lattice around the excited carriers. The A2 band is nonetheless on par in terms of intensity with the BE bleach, suggesting it arises from a strongly allowed transition and questioning its assignment to a formally forbidden band partially allowed by perturbation.

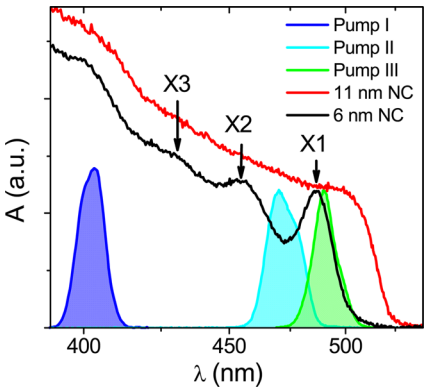

Figure 1. Linear absorption spectra of 6 and 10 nm $CsPbBr_3$ NCs, along with power spectra of the 3 excitation pulses used in the TA experiments.

In another recent study, TA was used to follow biexciton recombination rates in QC $CsPbBr_3$ NCs as a function of size.[24] As in numerous earlier NC studies,[10,25] Auger recombination (AR) rates were deduced from decay kinetics of the BE bleach as a function of pump−probe delay at substantial pump fluences where multiexcitons are deposited by sequential multiple photon absorption. Aside from demonstrating the relatively rapid AR rates in MLHP NCs, contrary to some earlier reports,[26] this experiment confirmed the expected $1/V$ (V = volume of NCs) dependence of k_{Auger} for the QC samples.[24] Interestingly, the amplitude ratio of the biexciton to single exciton bleaching signals did not follow the expected linear dependence reflecting integer BE state degeneracies.[24] These have been extensively debated, with claims of a dark or bright lowest exciton state.[27−29] However, consensus is growing that in MLHP NDs, the conduction and valence band edges consist of a single level significantly isolated in an energy space which is only spin degenerate.[30,31] In such a scenario expectations are for a symmetric state filling effect from both bands, with a linear increase of the BE bleach for the first two excitons, with the first transforming the sample from absorption to transparency and the second generating stimulated emission of the same intensity as the initial absorption. Together with the unusual appearance of A2, these observations demonstrate that much still remains to be understood concerning the electronic structure of QC MLHP NCs. What fraction of the BE absorption band is blocked by a single relaxed exciton, and how do valence and conduction band carriers contribute to state filling? What does this predict for another exciton, and do biexciton signatures in TA behave accordingly? In other words, does the bleach of the BE absorption present us with a reliable "exciton counter" for the first two excitons, and if not, then why? To answer these questions, we have studied state filling effects on the BE bleach for the first two deposited excitons in strongly QC $CsPbBr_3$ NDs using two and three pulse broad-band femtosecond TA. Biexciton contributions to TA spectra were isolated and compared to that induced by a single excitation using the "spectator exciton" approach.[8,32] Results show that besides induction of A2, a single exciton totally bleaches the initial $1S_e1S_h$ absorption band and that a second exciton does not change the bleach at the BE, but instead initially bleaches A2, proving it to be an extensively blue-shifted remaining transition to $1S_e1S_h$ and not a partially allowed dark band. Later, a picosecond range relaxation process in the nascent biexciton induces a back shift in the position of its induced bleach, partially reviving A2. These results are discussed in terms of a mechanistic scheme below and demonstrate that in MLHP NCs, the BE bleaching signal is not linear in the exciton number even for the first two absorbed photons and is thus not a reliable measure of the exciton number state.

RESULTS AND DISCUSSION

Figure 1 presents linear absorption spectra for two of the four oleic acid and oleylamine capped $CsPbBr_3$ NC samples studied. The sizes determined from transmission electron microscopy (TEM) (Figure S1) were 6 (±0.7) nm and 10 (±3) nm. As the Bohr diameter of the $CsPbBr_3$ NCs is 7 nm,[33] the carriers in the 6 nm CPB NCs experienced strong quantum confinement. At 10 nm, the particles whose absorption spectrum is plotted in red were very weakly effected by confinement. As expected for QC NCs, the BE exciton transition X1 and two higher bands designated as X2 and X3 are well resolved for the QC sample. In contrast, absorption peaks are not well resolved for the larger 10 nm particles, as expected for weakly confined particles. Characteristic TEM images and optical absorption spectra for 4.2 and 5 nm sided QC NCs are shown in Figures S1 and S2, demonstrating continued blue shifting of X1 with the decrease of the particle size. The luminescence spectra and quantum yields (QYs) of all four samples are shown in Figure S3. The high QYs demonstrate that the permanent carrier trapping is not active in these particles.

Pump−probe scans were recorded for 6 nm QC $CsPbBr_3$ NCs with excitation at 400 nm to follow carrier state-filling effects on the sample absorption, and test compatibility with earlier published data.[20] Figure 2A presents low fluence

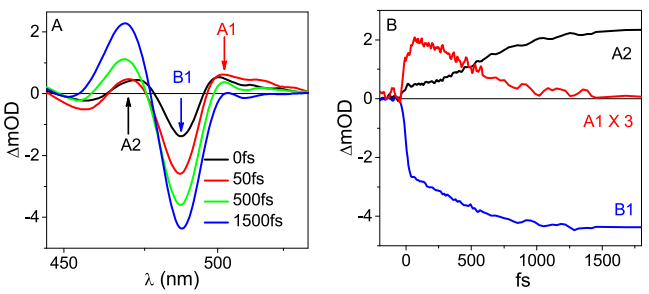

Figure 2. (A) TA spectra of 6 nm $CsPbBr_3$ particles at different time delays after low intensity pumping at 400 nm. (B) Spectral cuts at the central frequencies of B1 (~488 nm), A1 (~505 nm), and A2 (~470 nm).

https://doi.org/10.1021/acsnano.1c02123
ACS Nano XXXX, XXX, XXX−XXX

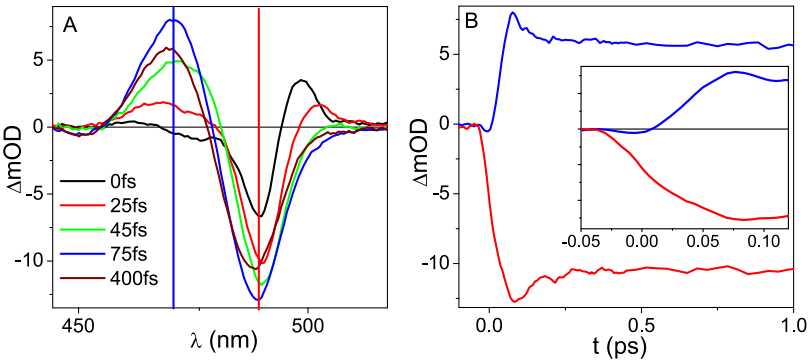

Figure 3. (A) Pump−probe spectra of 6 nm $CsPbBr_3$ particles at early time delays after pumping at the BE with pump spectrum III, Figure 1. (B) Spectral cuts at the center of B1 (red) and A2 (blue), designated by appropriately colored vertical lines in (A). Inset in (B): Same on an expanded time scale.

pump−probe transient spectra at a series of delays covering the process of carrier cooling. At this pump power, the data are dominated by singly excited particles. Spectra in panel A show the early rise in the A1 and B1 bands, followed by a slower rise in the BE bleach which takes place on a similar time scale as the rise in A2. As these changes occur, the below BE-induced absorption A1 also subsides. To demonstrate the kinetics of these changes, temporal cuts in the data at the three wavelengths designated in panel A are depicted in B, demonstrating the similarity of time scale for the three changes which are complete within the first 1.5 ps of pump−probe delay. These results are similar to findings of Rossi *et al.*[20] One notable discrepancy is the absence of any obvious delay in the appearance of A2 with respect to carrier cooling, noted in the earlier report to be several hundreds of fs, presumably due to a lattice deformation similar to that involved in polaron formation. Figure 2 shows no obvious delayed activation of A2 beyond hot carrier cooling. The same pump−probe scans for 4.2 and 5 nm particles were recorded and explained in Figures S4 and S5, respectively.

In order to disentangle these processes, TA experiments were conducted with pump pulses characterized by excitation pump spectrum III (Figure 1) which overlaps exclusively with X1 and thus avoids the stage of carrier cooling. Results of this experiment are presented in a similar two panel overlay in Figure 3. It is noteworthy that the instrument response function (IRF) in this experiment is ∼50 fs fwhm, so only the last two spectra in Figure 3A cleanly succeed the pump−probe overlap. The rise of B1 is not accompanied by that of a concomitant A1, and both B1 and A2 rise much faster than in Figure 2, as expected for direct population of the $1S_e1S_h$ exciton state. Interestingly there is a distinct difference in the rise of both bands. At the peak of pump−probe overlap ($t = 0$), B1 is in a first phase of buildup which lasts nearly the full IRF defined by pump and probe cross correlation. During this phase, A2 rises negligibly. This is followed by a second phase which sees the full rise in A2 and a near doubling of B1. Time resolution in this experiment IRF is not sufficient to fully separate these two stages, but a derivative of the B1 signal demonstrates this unmistakably (Figure S6). Thus, while the A2 band does appear slightly delayed with respect to population of the BE exciton state, once isolated in this fashion, its growth is much faster than previously reported.[20] A 15% decay of both these features within another 200 fs follows before the stabilizing of the signal for the full 200 ps of probe delay recorded. As seen in the Figure 3A, this later decay is the result of a blue shift in the bleach component of the spectrum producing an area conserving partial cancellation of the positive and negative lobes of this difference spectrum.

In order to quantify the fractional bleach introduced by a single relaxed exciton, the TA signals were recast as wavelength-dependent single particle differential cross sections ($\Delta\sigma$) and compared with the cross section of a pristine NC (σ). The latter has been derived by others for similar samples from spectrophotometry and chemical analysis to determine NC concentration[7,18] and/or by saturation analysis of fluence-dependent TA.[7] Here we use bleach saturation following multiexciton recombination for this purpose. Saturation experiments described graphically in Figure 4 (and Figure S7) were conducted by above band gap pumping at 400 nm where the absorbance of a NC is nearly insensitive to the first few photons already absorbed, validating the assumption of Poisson exciton statistics. Once the cross section at 400 nm is determined, that at other wavelengths can be calculated from the linear absorption spectrum like that in Figure 1. As

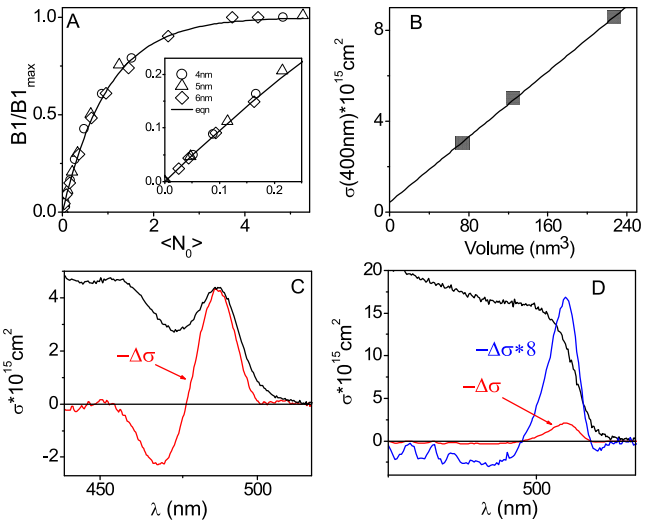

Figure 4. (A) BE bleach saturation as a function of N_0 ($=\rho^*\sigma$) following pumping at 400 nm. Inset: Linear portion of the saturation curves at low N_0. (B) Absorption cross sections (σ) obtained by fits summarized in (A) as a function of volume of the NCs along with a linear fit. Comparison of absorption cross section spectrum (black) with bleach difference cross section per exciton (red) for 6 nm (C) and 10 nm (D). Blue is amplification of $-\Delta\sigma$ for 10 nm particles for clarity.

https://doi.org/10.1021/acsnano.1c02123
ACS Nano XXXX, XXX, XXX−XXX

explained in the SIO, after AR has reduced all multiexcitons to singly excited particles, the amplitude of B1 scales as $B1/B1_{MAX} \cong 1 - \exp(-N_0)$, where N_0 represents the average number of excitons absorbed per NC which is the product of the measurable pump photon density per unit area, ρ, with the cross section σ. $B1_{MAX}$ is the asymptotic BE bleach amplitude at high fluence after AR. So while the NCs are assumed to continue absorbing the pump at 400 nm with the same cross section leading to a Poissonian distribution of excitations, B1 saturates as we approach the limit where all particles have absorbed at least one photon, leading to a uniform population of cold monoexcitons after AR. This leaves σ as a single free parameter for fitting the measured $B1/B1_{MAX}$ (ρ) data. This equation can be extended to incorporate the effects of pump depletion in optically thick samples. We have verified that just replacing ρ with the average pump photon density $\langle\rho\rangle$ is sufficient for covering these effects in our samples for which OD (400 nm) ~ 0.2.

Figure 4A presents the resulting fits for three QC samples of 6, 5, and 4.2 nm sided crystals as a function of N_0 for the best fitting values of σ each. Fitting was conducted independently for each sample, and the resulting optimal cross sections are presented as a function of the mean particle volumes in Figure 4B. This graph demonstrates the perfect linear correlation between σ and V within our experimental errors. These cross sections are inexplicably ~40% smaller than previously determined for identical NCs of the same sizes.[7,18] It is noteworthy that even if there were a systematic error in the determination of ρ, this would not impede comparison with pump–probe data since the same set of pinholes and power meters are used for characterizing pump fluences in TA measurements as well.

Figure 4C,D present the change in cross section induced by absorption of a single photon together with the cross section of the same sample for QC NCs (C) and the bulk-like sample (D). The wavelength dependent change in cross section per absorbed exciton, $\Delta\sigma(\lambda)$, is calculated from a low pump fluence TA spectrum after carrier cooling, $\Delta OD(\lambda)$, ensuring that $N_0 \ll 1$. Knowing further that $10^{-\Delta OD} = e^{-\Delta\sigma\times\theta}$, where θ is the density per unit area of absorbed photons (singly excited particles) derived from sample absorbance and pump fluence, we rearrange to $\Delta\sigma(\lambda) = 2.3\,\Delta OD(\lambda)/\theta$. This can be directly compared with $\sigma(\lambda)$ as shown in Figure 4C for the 6 nm sample (equivalent plots are presented for the other QC samples in the Figure S8). Figure 4C shows that aside from some discrepancies on the wings of the BE transition, a single exciton bleaches the $1S_e1S_h$ absorption band completely. In contrast, the ratio between the single exciton bleach and the initial step-like rise at the optical band gap for our bulk like sample is ~1/8. This is not far from the volume ratio of an exciton in $CsPbBr_3$ (~180 nm^3) to that of an average particle (~1000 nm^3).

Having a single exciton bleach, the BE peak is consistent with the electronic level scheme mentioned above, but this scheme does not predict the buildup of the A2 absorption band. To further our understanding of inorganic perovskite NC photophysics at the QC limit requires an extension of investigation beyond monoexciton. The highest intensity experiments from which saturation data presented in Figure 4A was obtained involve pump fluences inducing $N_0 > 4$. According to Poisson statistics, this leads to a dominant fraction of the population containing several excitons. In samples with edges ≤6 nm, the recombination in particles with three excitons or more is so fast that for excitation at 400 nm, it should take place in parallel with hot carrier cooling. Thus, the highest relaxed multiexciton state that can be observed in our experiment is the biexciton.

To estimate the effect of an additional exciton on the NC absorption, we compare TA just after carrier cooling to that established after AR of the relatively long-lived biexcitons. Subtraction of the two spectra records the change upon reduction from two to a single relaxed BE exciton. In reality separation of time scales between the two processes is incomplete due to rapid AR both due to the NC size and the nature of the MLHP materials. At least for the 6 nm sample, it is sufficient for quantitative subtraction for samples excited to saturation with $N_0 \geq 3$. The result of such a subtraction for 6 and 4.2 nm samples is shown in Figure 5

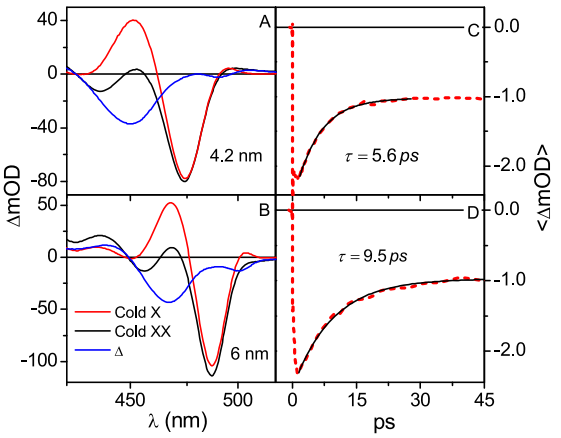

Figure 5. Cold biexciton (black) and cold single exciton (red) spectra following carrier cooling (at 1.2 ps) and Auger recombination (at 30 and 45 ps for 4.2 and 6 nm NCs, respectively), respectively, for 4.2 nm (A) and 6 nm (B) CPB NCs after 400 nm excitation. The blue one is the finite difference spectra of cold bi and monoexciton. Band integral over the range of A2 and B1 bands of 4.2 nm (C) and 6 nm (D) sized CPB NCs.

(Figure S9 for 5 nm samples). Contrary to expectations that a second exciton roughly doubles the effect of the first and transforms the doubly excited particle to stimulated emission at the BE, the second exciton has nearly no effect on TA at the BE. Instead, for both samples, the blue difference curves show that double excitation mainly bleaches the A2 band, along with what appears as a weak excess transmission on the red edge of the $1S_e1S_h$ feature.

The subtraction results in Figure 5 can explain the shallowness of bleach decays used to quantify AR rates in previous studies.[24] Indeed the 2:1 ratio expected for bleach signals at the B1 peak is not realized. A possible scenario is that A2 which arises rapidly after single excitation is actually an extensively blue-shifted remainder of the $1S_e1S_h$ absorption, which is accordingly bleached by another relaxed exciton. If so, the 2:1 ratio in the bleach signal anticipated for AR of the biexciton would be restored for an integral of the TA signal over a frequency range covering B1 and A2. Results of such band integrals, calculated as dipole strengths $\left(\Delta D \propto \int \frac{\Delta OD}{\upsilon} d\upsilon\right)$, are presented in Figure 5C,D for the 4.2 and 6 nm samples, respectively. Aside from reproducing the AR times of 5.6 and 9.5 ps for the two samples, both exhibit nearly a 2:1 ratio over the course of recombination, in

https://doi.org/10.1021/acsnano.1c02123
ACS Nano XXXX, XXX, XXX–XXX

accordance with A2 assigned to blue shifting of the band edge in the presence of an exciton.

To test this premise further, three pulse spectator exciton experiments (timing scheme is in Figure S10) were conducted on the 6 nm sample.[8,32] Briefly, the weak pump TA in a NC sample without any prior excitation is compared with an identical pump−probe cycle in the same sample after it has been saturated in relaxed monoexcitons. The first, as usual, measures changes in absorbance due to the addition of one exciton to a pristine NC, while the other records the changes of adding the next. It is based on the separation of time scales between AR of multiexcitons and radiative recombination which leaves an extensive temporal window for addressing a uniform sample of cold singly excited particles. Following the saturation with intense 400 nm pulses, pumping was performed near the peak of A2 for the 6 nm sample.

Figure 6 presents the results where panels A and B show overlays of 3 pulse TA spectra at various pump−probe delays

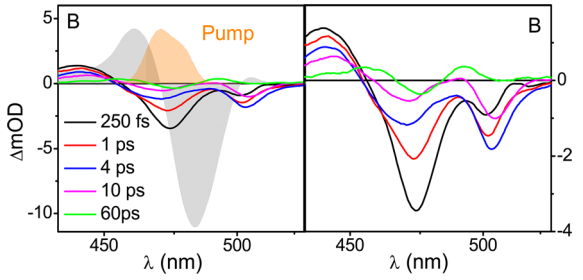

Figure 6. Left panel: Three pulse spectra at different time delays after pumping at 470 nm together with two pulse spectra at 250 fs (gray shaded) and pump intensity spectra. Right panel: Same three pulse spectra in expanded scale.

covering the recombination of nascent biexcitons generated by the pump. These are displayed on the shaded background of a 2 pulse TA spectrum obtained at a delay of 250 fs in panel A, and panel B presents the 3 pulse data alone on a narrower intensity range for clarity. Noteworthy observations in these experiments are, first, that the difference spectrum induced by the repumping of the sample decays back near zero amplitude with kinetics consistent with the AR rate of ~9.5 ps^{-1}. Second is the observation that band re-excitation leads to an induced bleach close to A2, and during recombination, a 2 state decay shifts the bleaching to the red of the BE. This is clarified by plotting the 3 pulse difference spectra over the initial 5 ps of delay after multiplication by $\exp(k_{Auger}t)$ in Figure S11, a factor which cancels the effect of Auger biexciton recombination and isolates the other dynamic processes.

Two different scenarios will be considered here to interpret the data. The first due to Rossi *et al.*[20] maintains that exciton-induced activation of a forbidden transition gives rise to the appearance of the A2 absorption band. The other assigns this absorption to a strong repulsive biexciton interaction in these NCs, up-shifting the remaining band edge carrier transitions after introduction of a first exciton by nearly 130 meV. Valuable information for evaluating these options is found in the AR experiments outlined in Figure 5. The biexcitons generated in these samples resulted from high fluence above band gap excitation, characterized with $N_0 \geq 4$. As shown in a previous report,[32] at such high N_0, spin blockades to hot exciton relaxation in the presence of additional BE excitons are relieved and a large majority of the biexcitons recorded have relaxed to the lowest available levels.[32] The fact that this leads not to a negative signal signifying strong stimulated emission matches the second scenario. In the first scenario discussed by Son and co-workers,[20] the second exciton would double the effect of the first on the BE transition regardless of perturbative allowing of transitions to a higher lying spin forbidden mixed exciton state. Restoration of a 2:1 ratio in the net bleach from band integrals shown in Figure 5C,D is also consistent with A2 stemming from blue shifting and not perturbation allowing, *etc.*

In order to delve deeper into AR data, TA spectra covering the process of cooling and recombination are presented in Figure 7 for the 6 nm sample (for similar analysis for the 4.2

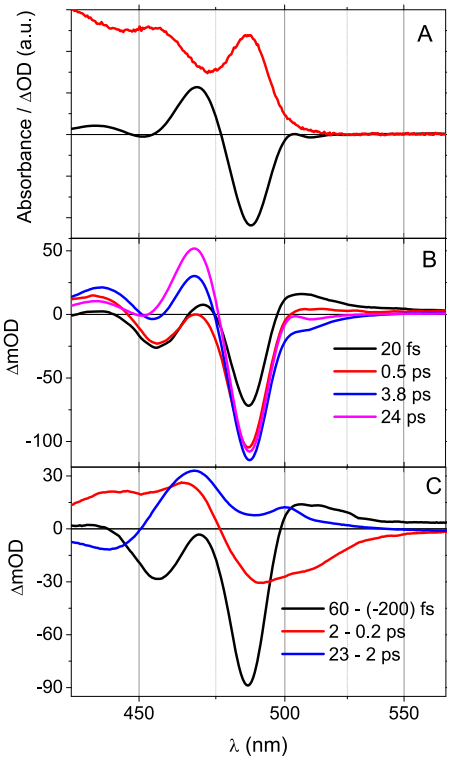

Figure 7. (A) Linear absorbance and change of absorbance following AR spectra of 6 nm CPB NCs after high intense 400 nm pump excitation. (B) Pump−probe spectra at different time delays of 6 nm CPB NCs following intense 400 nm pump excitation. (C) The finite difference spectral change for designated time intervals during cooling and AR after intense 400 nm pump excitation.

and 5 nm samples, see Figures S12 and S13). Figure 7A presents linear absorption as well as post-AR TA spectra for reference. TA evolution is presented as an overlay of spectra at particular delays during recombination in Figure 7B and finite difference spectra for designated delay ranges in Figure 7C. Finite difference spectra isolate TA evolution which takes place over a specific interval of pump−probe delays without interference from accumulating earlier spectral changes. Figure 7C reveals that, as in many other QC NCs, an effective separation of time scales exists between cooling and recombination in this sample. The earliest interval covers the prompt rise in bleaching of the BE exciton band, which is nearly complete within tens of femtoseconds. Despite exciting high above the band gap, the briefness of this buildup is surprising. Concentrating here on later stages of spectral change, the next phase spanning 0.2−2 ps is depicted in red and consists of the blue shifting of a broad initial absorption

https://doi.org/10.1021/acsnano.1c02123
ACS Nano XXXX, XXX, XXX−XXX

band surrounding B1, part of which induces the rapid decay of A1.

Integration of the red curve in Figure 7C indicates an underlying 475 nm centered absorption band 50 nm in width fwhm (see Figure S14). Similar changes in other NC samples[34] and specifically in MLHP thin layers are assigned to hot carrier cooling.[35] Here this must coincide with the recombination of higher multiexciton states as well, which are predicted to take place on a similar time scale. All the above set the stage for the latest phase of evolution, assignable to the AR of biexciton. This is observed most clearly in the blue curve and consists mainly of restoration of A2 which is complete within 25 ps. This portrayal of the sequence of events does not suggest strict sequentiallity, and recombination of multiexcitons must be taking place during cooling, *etc.* The effective separation of time scales still allows them to be effectively separated by finite spectral differencing.

The assignment of A2 to extreme blue shifting of the second BE transition poses several riddles. This shift is not only nearly an order of magnitude larger than biexciton interaction energies in other nanocrystals,[36,37] it is also opposite in sign or a repulsion. A similar situation has been observed in type II core/shell nanocrystals and promoted as a means of enhancing optical gain by relieving the overlap of emission and absorption at the mutual BG.[38,39] A possible mechanism which could simulate type II characteristics to the QC MLHP NCs is the segregation of electrons and holes due to lattice deformation and polaron formation. Indeed the formation of separate electron and hole-polarons would naturally cause segregation of the first carrier pair introduced by single photon absorption.[40,41] This would, however, not match the very brief appearance of band A2, which is barely observed even with the substantial time resolution achieved in these experiments. Reported time scales of ∼0.5 ps for polaron formation in bulk MHLPs match far better the stage we have collectively coined "cooling", although it must also involve the decay of higher multiexcitons.[40,41] The spectral signature of biexciton decay is strongly peaked at the A2 feature, demonstrating that most of its reappearance coincides with AR, even though some also appear to be taking place at earlier delays coinciding with carrier cooling as well. We also note that several studies have experimentally quantified biexciton interactions in QC MLHP NCs.[42,43] They neither agree between them nor with our findings on absolute magnitude nor even the sign of this interaction. It is, however, difficult to compare these with our own data since their samples are missing a distinct exciton structure, like that in Figure 1, and include biexciton interaction values derived from low time resolution time-resolved photoluminescence incapable of capturing AR dynamics in such small particles.

Another riddle concerns the amplitude of bleaching and scarceness of the net stimulated emission exhibited in Figure 7. The idea of devising biexciton repulsion in complex nanostructures is aimed at freeing stimulated emission from overlapping absorption.[38,39] But although such repulsion seems to exist in this single component NC, the integral BE bleach equals only half of the initial $1S_e1S_h$ absorption band, the full absorbance being bleached only at the biexciton level. If, as predicted theoretically, states at the edges of the conduction and valence bands are both exclusively spin degenerate,[27,44] hole filling effects from both would be expected to be equivalent and stimulated emission to be very clear even in TA of the monoexciton once the absorption to the biexciton is spectrally shifted to the blue. The observed behavior is very similar to the case of CdSe NCs where, for reasons which remain debated, BE hole state occupation does not bleach the $1S_e1S_h$ exciton band.[45,46] In MLHP, it is not clear in which band state filling effects are lacking, and this result is inconsistent with a scavenging study by Lian and co-workers which shows that in similarly sized NCs, extraction of electrons or holes by molecular scavengers leads to elimination of 70% and 30% of the BE bleach in TA experiments, respectively.[47] Further study will be required to determine why the expected equivalent effect of valence and conduction state filling is not realized and to understand why the effective integral biexciton bleach is only equal to the initial $1S_e1S_h$ absorption. It is noteworthy that, as in ref 45, even with the high time resolution 2 and 3 pulse pump−probe employed here, no initial signs of net emission were observed for biexciton, ruling out carrier trapping as a likely explanation for its curious absence.

We stress that while band integrals have been calculated in the range of 450−520 nm, significant overlap is apparent in the spectra of nearly all of the exciton peaks, and thus a perfect separation of spectral changes due to specific transitions is not possible. Some previous reports have assumed that spectra of NCs near the BG could be reproduced by fitting to a superposition of discrete Gaussian bands characterizing absorption or changes thereof to the first few exciton states.[48,49] Still others have assumed the gradual buildup of a continuum-like background band.[50,51] Since state filling should effect both, quantitative isolation assumed in the band integral approach is not possible. Indeed the A2 absorption peak coincides with the positive half of an apparent exciton-induced red shifting of the $1P_e1P_h$ peak, possibly responsible for a slight extension of the integral ratio above the ideal value of 2. Within these limitations, the near quantitative ratio results are taken as a strong justification of assigning A2 to biexciton repulsion specific to this material, a repulsion which may be applied in the future to boost lasing applications of QC perovskite NCs.

CONCLUSIONS

Absolute intensity broadband transient absorption measurements including three pulse "spectator exciton" scans on quantum confined $CsPbBr_3$ nanocrystals of various sizes have characterized the spectral dynamics of biexciton before and during Auger recombination. These demonstrate that a single exciton completely bleaches the band edge absorption peak and induces a new absorption roughly two times weaker ∼100 meV to the blue. Difference spectra obtained during Auger recombination of biexciton demonstrate that the addition of a second exciton, rather than double the effect of a first, bleaches the blue-induced absorption band without producing a net stimulated emission at the band edge. Accompanied by high time resolution TA spectra pumping at the lowest exciton band, these results identify the blue-induced absorption as the second transition to the 1Se1Sh exciton level which is shifted in energy due to unusually strong and promptly rising biexciton repulsion. At the same time, despite this strong repulsion, neither mono- nor biexcitons exhibit net stimulated emission, suggesting that hole and electron state filling does not equally effect bleaching of the band edge exciton absorption. Further study will be required to identify the mechanism giving rise to this strong biexciton repulsion and

https://doi.org/10.1021/acsnano.1c02123
ACS Nano XXXX, XXX, XXX−XXX

assessing its potential applications in achieving optical gain in quantum confined perovskite nanocrystals.

EXPERIMENTAL SECTION

Synthesis of Different Sized $CsPbBr_3$ NCs. *Chemicals.* Cesium carbonate (Cs_2CO_3, 99.9%, Sigma-Aldrich), lead(II) bromide ($PbBr_2$, ≥98%, Sigma-Aldrich), zinc(II) bromide ($ZnBr_2$ 99.999% m.b, Holland-Moran) oleic acid (OA, 90%, Sigma-Aldrich), oleylamine (OLAM, 70%, Sigma-Aldrich), 1-octadecene (ODE, 90%, Sigma-Aldrich), ethyl acetate (≥99.5%, Sigma-Aldrich), and hexane (not pure, Gadot) were purchased and used as received, without any further purification.

Preparation of Cs-Oleate. The Cs-oleate precursor was prepared according to a previously published procedure by Dong *et al.*[17] In a 100 mL 3-neck flask, 0.25g of Cs_2CO_3 (0.76 mmol) was mixed with 900 μL of OA and 9 mL of ODE. The solution was degassed for 1 h under vacuum conditions at 120 °C and then heated to 150 °C under an argon flow.

Synthesis of $CsPbBr_3$ NPs. The NPs were synthesized according to Dong *et al.*[17] First, 0.2 mmol of $PbBr_2$ was mixed with 0.7 mmol of $ZnBr_2$, 0.5 mL of OA, 0.5 mL of OLA, and 5 mL of ODE in an additional 100 mL 3-neck flask. The solution was degassed for 1 h under vacuum at 120 °C and then heated to 140−190 °C (for different size) under an argon flow. The reaction was carried out by injecting 0.4 mL of the Cs-oleate precursor solution into the $PbBr_2$ precursor solution using a preheated syringe. The reaction was quenched using an ice bath after a few seconds. Ethyl acetate was added to the crude solution in a volume ratio of 3:1, the NCs were centrifuged at 6000 rpm for 10 min, the participate was dispersed in hexane, and the NCs dispersion was centrifuged again at 3000 rpm for 5 min to get rid of aggregates and unreacted salts.

High-resolution Transmission Electron Microscopy. Morphology of the NPs was analyzed with a Tecnai F20 G2 (FEI Company, USA) high-resolution transmission electron microscope. Samples preparation was performed as follows: 2.5 μL of the NCs dispersion was dropped on an ultralight copper grid coated with amorphous carbon film.

Femtosecond Pump−Probe Measurements. To perform the pump−probe measurement, the samples were placed in a 0.5 mm airtight quartz cell in an inert atmosphere inside the glovebox. The home-built TA setup was appointed for the TA measurement. The fundamental 790 nm pulses with ∼35 fs pulse width and 1 mJ energy per pulse at 1 kHz repetition rate were generated by the multipass amplified Ti-sapphire laser system. The generated 790 fundamental pulses were split to generate the pump and probe pulses. The fundamental 790 nm pulses produced the 400 nm pump pulses by frequency doubling inside the BBO crystal. The 470 and 490 nm pulses were produced from optical parametric amplifier (TOPAS Prime) and were compressed by the grating-mirror compressor setup. The white light continuum probe pulses (400−700 nm) were generated by focusing the 790 nm fundamental pulses on the 2 mm CaF2 crystals. No dispersive medium was used on the pump and probe path to avoid the extra chirp. On the sample, the spot size of the pump pulses was at least three times larger than the probe pulse. We used the rotating optical cell to avoid the charging process of the sample.

In the conventional two pulse measurement, the samples were excited by the 400/470/490 nm pump pulse with weak intensity to avoid the multiexciton generation or varying the intensity and probed by the 400−700 nm white-light continuum. To measure the absorption cross-section and bleach cross-section per exciton very precisely, the samples were excited by the 400 nm pump. In three pulse measurement, the same two pulse measurement was repeated in the presence of single cold exciton in every particle produced by the 400 nm intense pump following AR. The intense 400 nm pulse excited the material ∼50 ps earlier than the second pump and generated the maximum possible number of excitons at the band edge. For both two- and three pulse measurements, the probe pulses were exposed to the SpectraPro 2150i imaging spectrograph (Acton Research Corporation) equipped with a CCD camera (Entwicklungsbüro Stresing).

ASSOCIATED CONTENT

Supporting Information

The Supporting Information is available free of charge at https://pubs.acs.org/doi/10.1021/acsnano.1c02123.

Detailed characterization of different sized $CsPbBr_3$ NCs by HR-TEM, optical absorption and emission spectra with QY, TA spectra and spectral cuts of 4.2 and 5 nm CPB NCs, derivative of band edge bleach rise, calculation of absorption cross-section at 400 nm and bleach cross-section per exciton from TA study, single and biexciton spectra for 5 nm CPB NCs, 400−470 nm WL three pulse studies (scheme and spectra), higher pump intensity studies for 4.2 and 5 nm CPB NCs, integration of finite difference spectra of 2−0.2 ps for 6 nm CPB NCs (PDF)

AUTHOR INFORMATION

Corresponding Author

Sanford Ruhman − *Institute of Chemistry, The Hebrew University of Jerusalem, Jerusalem 91904, Israel;* orcid.org/0000-0003-0575-1367; Email: sandy@mail.huji.ac.il

Authors

Jayanta Dana − *Institute of Chemistry, The Hebrew University of Jerusalem, Jerusalem 91904, Israel*

Tal Binyamin − *Institute of Chemistry, The Hebrew University of Jerusalem, Jerusalem 91904, Israel*

Lioz Etgar − *Institute of Chemistry, The Hebrew University of Jerusalem, Jerusalem 91904, Israel;* orcid.org/0000-0001-6158-8520

Complete contact information is available at: https://pubs.acs.org/10.1021/acsnano.1c02123

Notes

The authors declare no competing financial interest.

This article was submitted to ChemRxiv preprint server: Dana, J.; Binyamin, T.; Etgar, L.; Ruhman, S. Unusually Strong Biexciton Repulsion Detected in Quantum Confined $CsPbBr_3$ Nanocrystals with Two and Three Pulse Femtosecond Spectroscopy. *ChemRxiv*, March 11, 2021 ver. 1. 10.26434/chemrxiv.14191454.v1 (accessed 2021-03-11).

ACKNOWLEDGMENTS

S.R. acknowledges funding from the ISF (grant 163/16), which is administered by the Israeli Academy of Sciences, and holds the Aronberg Chair in Chemistry. J.D. acknowledges support from the PBC fellowship program of the Israeli council for higher education. L.E. acknowledges the Israel Science Foundation grant number: 937/18.

REFERENCES

(1) Brus, L. E. Electron−Electron and Electron-Hole Interactions in Small Semiconductor Crystallites: The Size Dependence of the Lowest Excited Electronic State. *J. Chem. Phys.* **1984**, *80*, 4403−4409.

(2) Efros, Al. L.; Rosen, M.; Kuno, M.; Nirmal, M.; Norris, D. J.; Bawendi, M. Band-Edge Exciton in Quantum Dots of Semiconductors with a Degenerate Valence Band: Dark and Bright Exciton States. *Phys. Rev. B: Condens. Matter Mater. Phys.* **1996**, *54*, 4843−4856.

(3) Talapin, D. V.; Lee, J.-S.; Kovalenko, M. V.; Shevchenko, E. V. Prospects of Colloidal Nanocrystals for Electronic and Optoelectronic Applications. *Chem. Rev.* **2010**, *110*, 389−458.
(4) Kim, J. Y.; Voznyy, O.; Zhitomirsky, D.; Sargent, E. H. 25th Anniversary Article: Colloidal Quantum Dot Materials and Devices: A Quarter-Century of Advances. *Adv. Mater.* **2013**, *25*, 4986−5010.
(5) Yang, Y.; Zheng, Y.; Cao, W.; Titov, A.; Hyvonen, J.; Manders, J. R.; Xue, J.; Holloway, P. H.; Qian, L. High-Efficiency Light-Emitting Devices Based on Quantum Dots with Tailored Nanostructures. *Nat. Photonics* **2015**, *9*, 259.
(6) Kambhampati, P.; Mi, Z.; Cooney Ryan, R. Colloidal and Self-Assembled Quantum Dots for Optical Gain. *In Comprehensive Nanoscience and Technology;* Andrews, D. L., Scholes, G. D., Wiederrecht, G. P., Eds.; Academic Press: Oxford, 2011; pp 493−542.
(7) Klimov, V. I. Optical Nonlinearities and Ultrafast Carrier Dynamics in Semiconductor Nanocrystals. *J. Phys. Chem. B* **2000**, *104*, 6112−6123.
(8) Gdor, I.; Shapiro, A.; Yang, C.; Yanover, D.; Lifshitz, E.; Ruhman, S. Three-Pulse Femtosecond Spectroscopy of PbSe Nanocrystals: 1S Bleach Nonlinearity and Sub-Band-Edge Excited-State Absorption Assignment. *ACS Nano* **2015**, *9*, 2138−2147.
(9) Puthenpurayil, J.; Cheng, O. H.-C.; Qiao, T.; Rossi, D.; Son, D. H. On the Determination of Absorption Cross Section of Colloidal Lead Halide Perovskite Quantum Dots. *J. Chem. Phys.* **2019**, *151*, 154706.
(10) Klimov, V. I. Multicarrier Interactions in Semiconductor Nanocrystals in Relation to the Phenomena of Auger Recombination and Carrier Multiplication. *Annu. Rev. Condens. Matter Phys.* **2014**, *5*, 285.
(11) Ben-Lulu, M.; Mocatta, D.; Bonn, M.; Banin, U.; Ruhman, S. On the Absence of Detectable Carrier Multiplication in a Transient Absorption Study of InAs/CdSe/ZnSe Core/Shell1/Shell2 Quantum Dots. *Nano Lett.* **2008**, *8*, 1207−1211.
(12) Huang, J.; Huang, Z.; Yang, Y.; Zhu, H.; Lian, T. Multiple Exciton Dissociation in CdSe Quantum Dots by Ultrafast Electron Transfer to Adsorbed Methylene Blue. *J. Am. Chem. Soc.* **2010**, *132*, 4858−4864.
(13) Trinh, M. T.; Houtepen, A. J.; Schins, J. M.; Piris, J.; Siebbeles, L. D. A. Nature of the Second Optical Transition in PbSe Nanocrystals. *Nano Lett.* **2008**, *8*, 2112−2117.
(14) Labrador, T.; Dukovic, G. Simultaneous Determination of Spectral Signatures and Decay Kinetics of Excited State Species in Semiconductor Nanocrystals Probed by Transient Absorption Spectroscopy. *J. Phys. Chem. C* **2020**, *124*, 8439−8447.
(15) Ghosh, T.; Aharon, S.; Shpatz, A.; Etgar, L.; Ruhman, S. Reflectivity Effects on Pump−Probe Spectra of Lead Halide Perovskites: Comparing Thin Films *versus* Nanocrystals. *ACS Nano* **2018**, *12*, 5719−5725.
(16) Geiregat, P.; Maes, J.; Chen, K.; Drijvers, E.; De Roo, J.; Hodgkiss, J. M.; Hens, Z. Using Bulk-Like Nanocrystals to Probe Intrinsic Optical Gain Characteristics of Inorganic Lead Halide Perovskites. *ACS Nano* **2018**, *12*, 10178−10188.
(17) Dong, Y.; Qiao, T.; Kim, D.; Parobek, D.; Rossi, D.; Son, D. H. Precise Control of Quantum Confinement in Cesium Lead Halide Perovskite Quantum Dots *via* Thermodynamic Equilibrium. *Nano Lett.* **2018**, *18*, 3716−3722.
(18) Maes, J.; Balcaen, L.; Drijvers, E.; Zhao, Q.; De Roo, J.; Vantomme, A.; Vanhaecke, F.; Geiregat, P.; Hens, Z. Light Absorption Coefficient of $CsPbBr_3$ Perovskite Nanocrystals. *J. Phys. Chem. Lett.* **2018**, *9*, 3093−3097.
(19) Zhang, B.; Goldoni, L.; Lambruschini, C.; Moni, L.; Imran, M.; Pianetti, A.; Pinchetti, V.; Brovelli, S.; De Trizio, L.; Manna, L. Stable and Size Tuneable $CsPbBr_3$ Nanocrystals Synthesized with Oleylphosphonic Acid. *Nano Lett.* **2020**, *20*, 8847−8853.
(20) Rossi, D.; Wang, H.; Dong, Y.; Qiao, T.; Qian, X.; Son, D. H. Light-Induced Activation of Forbidden Exciton Transition in Strongly Confined Perovskite Quantum Dots. *ACS Nano* **2018**, *12*, 12436−12443.
(21) Sewall, S. L.; Franceschetti, A.; Cooney, R. R.; Zunger, A.; Kambhampati, P. Direct Observation of the Structure of Band-Edge Biexcitons in Colloidal Semiconductor CdSe Quantum Dots. *Phys. Rev. B: Condens. Matter Mater. Phys.* **2009**, *80*, 081310.
(22) Klimov, V. I.; McBranch, D. W. Femtosecond 1 P -to- 1 S Electron Relaxation in Strongly Confined Semiconductor Nanocrystals. *Phys. Rev. Lett.* **1998**, *80*, 4028−4031.
(23) Kambhampati, P. Hot Exciton Relaxation Dynamics in Semiconductor Quantum Dots: Radiationless Transitions on the Nanoscale. *J. Phys. Chem. C* **2011**, *115*, 22089−22109.
(24) Li, Y.; Ding, T.; Luo, X.; Chen, Z.; Liu, X.; Lu, X.; Wu, K. Biexciton Auger Recombination in Mono-Dispersed, Quantum-Confined $CsPbBr_3$ Perovskite Nanocrystals Obeys Universal Volume-Scaling. *Nano Res.* **2019**, *12*, 619−623.
(25) Kong, D.; Jia, Y.; Ren, Y.; Xie, Z.; Wu, K.; Lian, T. Shell-Thickness-Dependent Biexciton Lifetime in Type I and Quasi-Type II CdSe@CdS Core/Shell Quantum Dots. *J. Phys. Chem. C* **2018**, *122*, 14091−14098.
(26) Makarov, N. S.; Guo, S.; Isaienko, O.; Liu, W.; Robel, I.; Klimov, V. I. Spectral and Dynamical Properties of Single Excitons, Biexcitons, and Trions in Cesium−Lead-Halide Perovskite Quantum Dots. *Nano Lett.* **2016**, *16*, 2349−2362.
(27) Becker, M. A.; Vaxenburg, R.; Nedelcu, G.; Sercel, P. C.; Shabaev, A.; Mehl, M. J.; Michopoulos, J. G.; Lambrakos, S. G.; Bernstein, N.; Lyons, J. L.; Stöferle, T.; Mahrt, R. F.; Kovalenko, M. V.; Norris, D. J.; Rainò, G.; Efros, A. L. Bright Triplet Excitons in Caesium Lead Halide Perovskites. *Nature* **2018**, *553*, 189−193.
(28) Rossi, D.; Liu, X.; Lee, Y.; Khurana, M.; Puthenpurayil, J.; Kim, K.; Akimov, A. V.; Cheon, J.; Son, D. H. Intense Dark Exciton Emission from Strongly Quantum-Confined $CsPbBr_3$ Nanocrystals. *Nano Lett.* **2020**, *20*, 7321−7326.
(29) Fu, M.; Tamarat, P.; Huang, H.; Even, J.; Rogach, A. L.; Lounis, B. Neutral and Charged Exciton Fine Structure in Single Lead Halide Perovskite Nanocrystals Revealed by Magneto-Optical Spectroscopy. *Nano Lett.* **2017**, *17*, 2895−2901.
(30) Li, Y.; Luo, X.; Liu, Y.; Lu, X.; Wu, K. Size- and Composition-Dependent Exciton Spin Relaxation in Lead Halide Perovskite Quantum Dots. *ACS Energy Lett.* **2020**, *5*, 1701−1708.
(31) Strohmair, S.; Dey, A.; Tong, Y.; Polavarapu, L.; Bohn, B. J.; Feldmann, J. Spin Polarization Dynamics of Free Charge Carriers in $CsPbI_3$ Nanocrystals. *Nano Lett.* **2020**, *20*, 4724−4730.
(32) Ghosh, T.; Dehnel, J.; Fabian, M.; Lifshitz, E.; Baer, R.; Ruhman, S. Spin Blockades to Relaxation of Hot Multiexcitons in Nanocrystals. *J. Phys. Chem. Lett.* **2019**, *10*, 2341−2348.
(33) Protesescu, L.; Yakunin, S.; Bodnarchuk, M. I.; Krieg, F.; Caputo, R.; Hendon, C. H.; Yang, R. X.; Walsh, A.; Kovalenko, M. V. Nanocrystals of Cesium Lead Halide Perovskites ($CsPbX_3$, X = Cl, Br, and I): Novel Optoelectronic Materials Showing Bright Emission with Wide Colour Gamut. *Nano Lett.* **2015**, *15*, 3692−3696.
(34) Gdor, I.; Yang, C.; Yanover, D.; Sachs, H.; Lifshitz, E.; Ruhman, S. Novel Spectral Decay Dynamics of Hot Excitons in PbSe Nanocrystals: A Tunable Femtosecond Pump−Hyperspectral Probe Study. *J. Phys. Chem. C* **2013**, *117*, 26342−26350.
(35) Ghosh, T.; Aharon, S.; Etgar, L.; Ruhman, S. Free Carrier Emergence and Onset of Electron−Phonon Coupling in Methylammonium Lead Halide Perovskite Films. *J. Am. Chem. Soc.* **2017**, *139*, 18262−18270.
(36) Achermann, M.; Hollingsworth, J. A.; Klimov, V. I. Multiexcitons Confined within a Subexcitonic Volume: Spectroscopic and Dynamical Signatures of Neutral and Charged Biexcitons in Ultra Small Semiconductor Nanocrystals. *Phys. Rev. B: Condens. Matter Mater. Phys.* **2003**, *68*, 245302.
(37) Ellis, B. H.; Chakraborty, A. Investigation of Many-Body Correlation in Biexcitonic Systems Using Electron−Hole Multicomponent Coupled-Cluster Theory. *J. Phys. Chem. C* **2017**, *121*, 1291−1298.
(38) Klimov, V. I.; Ivanov, S. A.; Nanda, J.; Achermann, M.; Bezel, I.; McGuire, J. A.; Piryatinski, A. Single-Exciton Optical Gain in Semiconductor Nanocrystals. *Nature* **2007**, *447*, 441−446.

https://doi.org/10.1021/acsnano.1c02123
ACS Nano XXXX, XXX, XXX−XXX

(39) Avidan, A.; Oron, D. Large Blue Shift of the Biexciton State in Tellurium Doped CdSe Colloidal Quantum Dots. *Nano Lett.* **2008**, *8*, 2384−2387.
(40) Evans, T. J. S.; Miyata, K.; Joshi, P. P.; Maehrlein, S.; Liu, F.; Zhu, X.-Y. Competition between Hot-Electron Cooling and Large Polaron Screening in $CsPbBr_3$ Perovskite Single Crystals. *J. Phys. Chem. C* **2018**, *122*, 13724−13730.
(41) Bretschneider, S. A.; Ivanov, I.; Wang, H. I.; Miyata, K.; Zhu, X.; Bonn, M. Quantifying Polaron Formation and Charge Carrier Cooling in Lead-Iodide Perovskites. *Adv. Mater.* **2018**, *30*, 1707312.
(42) Castañeda, J. A.; Nagamine, G.; Yassitepe, E.; Bonato, L. G.; Voznyy, O.; Hoogland, S.; Nogueira, A. F.; Sargent, E. H.; Cruz, C. H. B.; Padilha, L. A. Efficient Biexciton Interaction in Perovskite Quantum Dots under Weak and Strong Confinement. *ACS Nano* **2016**, *10*, 8603−8609.
(43) Ashner, M. N.; Shulenberger, K. E.; Krieg, F.; Powers, E. R.; Kovalenko, M. V.; Bawendi, M. G.; Tisdale, W. A. Size-Dependent Biexciton Spectrum in $CsPbBr_3$ Perovskite Nanocrystals. *ACS Energy Lett.* **2019**, *4*, 2639−2645.
(44) Ramade, J.; Andriambariarijaona, L. M.; Steinmetz, V.; Goubet, N.; Legrand, L.; Barisien, T.; Bernardot, F.; Testelin, C.; Lhuillier, E.; Bramati, A.; Chamarro, M. Fine Structure of Excitons and Electron−Hole Exchange Energy in Polymorphic $CsPbBr_3$ Single Nanocrystals. *Nanoscale* **2018**, *10*, 6393−6401.
(45) Dana, J.; Haggag, O. S.; Dehnel, J.; Mor, M.; Lifshitz, E.; Ruhman, S. Testing the Fate of Nascent Holes in CdSe Nanocrystals with Sub-10 Fs Pump−Probe Spectroscopy. *Nanoscale* **2021**, *13*, 1982−1987.
(46) Klimov, V. I.; Schwarz, Ch. J.; McBranch, D. W.; Leatherdale, C. A.; Bawendi, M. G. Ultrafast Dynamics of Inter- and Intra-band Transitions in Semiconductor Nanocrystals: Implications for Quantum-Dot Lasers. *Phys. Rev. B: Condens. Matter Mater. Phys.* **1999**, *60*, R2177−R2180.
(47) Wu, K.; Liang, G.; Shang, Q.; Ren, Y.; Kong, D.; Lian, T. Ultrafast Interfacial Electron and Hole Transfer from CsPbBr3 Perovskite Quantum Dots. *J. Am. Chem. Soc.* **2015**, *137*, 12792−12795.
(48) Nandan, Y.; Mehata, M. S. Wavefunction Engineering of Type-I/Type-II Excitons of CdSe/CdS Core-Shell Quantum Dots. *Sci. Rep.* **2019**, *9*, 2.
(49) Kim, S. H.; Man, M. T.; Lee, J. W.; Park, K.-D.; Lee, H. S. Influence of Size and Shape Anisotropy on Optical Properties of CdSe Quantum Dots. *Nanomaterials* **2020**, *10*, 1589.
(50) Su, G.; Liu, C.; Deng, Z.; Zhao, X.; Zhou, X. Size-Dependent Photoluminescence of PbS QDs Embedded in Silicate Glasses. *Opt. Mater. Express* **2017**, *7*, 2194−2207.
(51) Zhang, C.; Do, T. N.; Ong, X.; Chan, Y.; Tan, H.-S. Understanding the Features in the Ultrafast Transient Absorption Spectra of CdSe Quantum Dots. *Chem. Phys.* **2016**, *481*, 157−164.

https://doi.org/10.1021/acsnano.1c02123
ACS Nano XXXX, XXX, XXX−XXX